Heliyon 10 (2024) e34435

Contents lists available at ScienceDirect

Heliyon

journal homepage: www.cell.com/heliyon

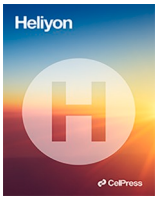

Research article

Pyrolysis of metal oxides treated *Canarium schweinfurthii* Shell: Investigation of thermogravimetric kinetics and thermodynamics

Kabir Garba [a,*], Habu Iyodo Mohammed [a,b], Yusuf Makarfi Isa [c]

[a] *Department of Chemical Engineering, Abubakar Tafawa Balewa University, P.M.B 0248, Bauchi, Nigeria*
[b] *Department of Chemical Engineering, University of Maiduguri, P.M.B 1069, Maiduguri, Nigeria*
[c] *School of Chemical and Metallurgical Engineering, University of the Witwatersrand, 1 Jan Smuts Avenue, Braamfontein, 2000, Johannesburg, South Africa*

ARTICLE INFO

Keywords:
Biomass
Canarium schweinfurthii fruit shell
Metal oxides
Kinetic
Pyrolysis
Thermogravimetric

ABSTRACT

Metal oxides as catalysts alter the properties of the pyrolysis vapor secondary reactions during the thermal decomposition of several biomass leading to high-value bio-oils. This study aimed to investigate the thermal decomposition characteristics of *Canarium Schweinfurthii* (CS) shells that were treated with various metal oxides (ZnO, CuO, Fe_2O_3/FeO, and Fe_2O_3) using pyrolysis. The study also sought to identify pyrolysis reaction parameters (kinetics and thermodynamics parameters) that are not widely documented. Thermogravimetric pyrolysis was carried out at different heating rates, and the undocumented pyrolysis kinetic parameters were determined using the Flynn-Wall Ozawa method (FWO) according to American Standard Testing and Materials (ASTM) 6441 guidelines for assessing biomass decomposition. The metal oxide-treated CS shells lost significant weight between 62 and 67 wt% during the thermogravimetric pyrolysis, lower than 75 wt% of the CS shell. The average activation energies (E_α) for pyrolysis of the ZnO, CuO, Fe_2O_3/FeO, and Fe_2O_3 treated CS shells were 203.04, 155.35, 338.85, and 219.92 kJ/mol, respectively in contrast to that of the untreated CS-shell. The Bayesian Information Criteria revealed that the diffusion kinetics of the Gistling-Brounshtein model best describes the pyrolysis of the shell mixed with metal oxides. The metal oxides affected the CS shells' pyrolysis kinetic parameter (E_α), which can promote pyrolysis vapor upgrading to encourage the widespread use of metal oxides in pyrolysis for bioenergy and chemical recovery.

1. Introduction

The increased need to harness the limited biomass available to produce value-added biofuel and chemicals demands the search for catalysts and technology that lower energy consumption, improve yields, and use high-value components.

Catalysts in situ with biomass not only direct pyrolysis vapor to high-value pyrolytic oil but also affect activation energy (E_α) and thermodynamic parameters for pyrolysis system operations [1]. Thermodynamics and kinetics of thermal decomposition of several biomasses have been investigated [2,3], such as Hyphaene Thebaica shell [3], Pongamia pinnata [4], palm kernel shell [5], Typha latifolia [6], *chlorella vulgaris* [7] and *Canarium Schweinfurthii* hard shell [8].

The effect of catalysts on the thermal decomposition of species of biomass has been previously reported in the literature [9,10].

* Corresponding author.
E-mail addresses: gkabir@atbu.edu.ng, kbgarba.1214@gmail.com (K. Garba).

https://doi.org/10.1016/j.heliyon.2024.e34435
Received 2 May 2024; Received in revised form 21 June 2024; Accepted 9 July 2024
Available online 10 July 2024

Effects of MgO, CaO, and ZnO on the activation energy of pyrolysis of Empty Palm Fruit Bunch (EFB) were investigated by Yee et al. [11]. These oxides lowered the E_α of EFB, where the most significant decrease was from 274.5 to 194.8 kJ/mol by treating the EFB with MgO (10 wt%). A separate study reported that catalytic pyrolysis of rice hull with calcium oxide derived from eggshell and limestone reduced the values of E_α [12]. Yang et al. [13] studied the catalytic effects of Ni–CaO–Ca_2SiO_3 and Ni–Ca_2SiO_3 on the pyrolysis of pine wood sawdust. A decrease in E_α, biomass pyrolysis produces H_2 and CO from the breakage of light organic molecules was observed. Wibowo et al. [9] investigated the effects of rice husk ash as catalysts in catalytic pyrolysis of rice husk. The E_α decreased with ash addition ratios. The addition of the catalyst slowed the decomposition of hemicellulose but accelerated the decomposition of cellulose and lignin. The *Canarium schweinfurthii* hard shell was studied for its thermochemical conversion to high-grade bioenergy precursors, in which the bio-oil derived by thermal pyrolysis yields complex phenolics and oxygenates [8]. The effects of catalysts on their thermos-kinetic behaviors were lacking.

There are several approaches to evaluating E_α and pre-exponential factors, which include Coats-Redfern, Flynn Wall Ozawa (FWO), Kissinger-Akhira-Sunose (KAS), and Starink methods [3,14]. Mohammed et al. [3] compared the FWO, KAS, and Starink methods to evaluate the kinetics and thermodynamics parameters of the thermogravimetric pyrolysis of the *hyphaene thebaica* shell. The FWO method best describes the process as the kinetic parameters obtained are accurate. Furthermore, Chee et al. [15], observed that the kinetic parameters determined using FWO, KAS, and Distributed Activation Energy Model (DEAM) for catalytic and co-pyrolysis of palm kernel shells and plastic wastes are consistent with the literature. Also, Gan et al. [12] found FWO more reliable than DEAM in determining kinetic parameters for catalytic pyrolysis of rice husk over limestone and eggshell catalysts. In addition, FWO is the method adopted by American Standard Testing and Materials (ASTM) 1641 for accurately examining biomass thermal decomposition properties. However, other numerical approaches, such as Artificial Neural Networks (ANN) are being investigated [7,12].

The catalytic pyrolysis of the CS shell might lead to the release of vapor, resulting in a high-value pyrolytic oil rich in phenol, aromatic acids, esters, and hydrocarbons. The challenge lies in identifying appropriate catalysts that lower energy consumption and direct the pyrolysis reaction mechanisms to favor selectivity toward value-added compounds. The activities of transition metals, such as nickel and iron oxide, in upgrading the pyrolysis vapor of some biomass species were investigated, and reported in the literature [16], nickel and iron oxide promote yields of monoaromatic hydrocarbons. Catalytic upgrading of pyrolysis oil derived from sawdust by natural gas at atmospheric pressure over Zn, Fe, Co, Cu, Ni, Mn, Zr, and Ce supported on ZSM-5 was investigated, Zn gives the highest oil yield, with a high oil H/C atomic ratio and a low oil O/C atomic ratio [17]. A study by Lugovoy et al. [18] reported that a composite of ZSM-5-bentonite and 2 % cobalt resulted in a high yield of gas rich in methane. Catalytic pyrolysis of cellulose using Zn/ZSM-5 and $FePO_4$/ZSM-5 caused the production of furan compounds and levoglucosan [19]. The current trend suggests cheaper resources as catalyst feedstock for bioenergy production through the thermochemical conversion of biomass [20]. Iron ore dust (IOD) from an iron ore milling site is a cheap source of iron oxides that can serve as a catalyst in catalytic pyrolysis processes for this study.

The Canarium Schweinfurthii (CS) nut is mass-produced and has a shell (CS-shell) enclosing its kernel that causes waste management concerns. This study aims to explore the thermogravimetric pyrolysis of the CS-shell with metal oxides (Fe_2O_3, ZnO, CuO, and mixed Fe_2O_3/FeO obtained from the decomposition of magnetite). The CS shells' pyrolysis properties with the selected metal oxides are yet to be documented. Therefore, it is crucial to perform a comprehensive investigation through the thermogravimetric pyrolysis of the CS-shell with the metal oxides. The metal oxides' catalytic activities can be predicted from kinetics and thermodynamic parameters obtained from thermogravimetric pyrolysis. The study explores various metal oxides to identify appropriate catalysts that lower energy consumption and direct the pyrolysis reaction mechanisms to favor selectivity towards value-added compounds.

2. Materials and methods

2.1. Materials, CS-shell preparation, and thermogravimetric pyrolysis

The *Canarium schweinfurthii* fruit shell was obtained from Plateau State, Nigeria. The reagent-grade Copper sulfate pentahydrate ($CuSO_4.5H_2O$), Zinc nitrate hexahydrate ($Zn(NO_3)_2.6H_2O$), and Iron sulfate heptahydrate ($FeSO_4.7H_2O$) salts were supplied by Sigma-Aldrich through a local chemical vendor in Lagos, Nigeria. Iron ore dust (IOD) rich with 84 wt% magnetite (Fe_3O_4) was collected from a mining site in Bauchi, Nigeria. An X-ray fluorescence spectrometer (Rigaku RIX 3000) with X-ray fluorescence (XRF) was used to reveal the composition of the raw and calcined IOD, as shown in Table 1. A chemical reagent vendor supplied N_2 (99.99 %) as a

Table 1
XRF compositions of Iron ore dust.

Compounds	Raw	Calcined @ 900 °C	Literature [21]
	(wt.%, dry basis)		
SiO_2	7.99	6.45	9.5
Al_2O_3	4.04	5.58	1.71
Fe_3O_4	83.58	–	37.5
Fe_2O_3	–	43.42	34.0
FeO	–	40.83	–
CaO	1.60	1.40	8.5
MgO	2.79	2.32	0.85
Others	0.00	0.00	7.94
Total	**100**	**100**	**100**

sweeping gas in thermogravimetric pyrolysis investigations.

2.2. Methods

2.2.1. Characterization and preparation of Canarium schweinfurthii shell

This study employed the same C*anarium schweinfurthi*i shell sample as in a previous study [8] for thermogravimetric pyrolysis studies on Shimadzu TGA 50. The CS-shell's proximate and ultimate analyses were performed on a thermogravimetric analyzer (PerkinElmer STA 6000) and a CHNO/S analyzer (PerkinElmer 400 Series II), respectively. The high heating value (HHV) was determined on an IKA C 200 bomb calorimeter.

At an equivalent weight of 10 wt%, the IOD and CS-Shell powder were monodispersed, while the hydrated metal salts were doped onto the CS-Shell. The thermogravimetric pyrolysis was performed at 10, 15, and 20 °C/min heating rates on the treated CS shells. The kinetic and thermodynamic parameters were determined using weight loss data. During the pyrolysis, the IOD, mostly 83.58 wt% magnetite (Fe_3O_4) decomposed into mixed iron oxide (Fe_2O_3/FeO). However, the doped metal salts decomposed into their respective metal oxides, ZnO, CuO, and Fe_2O_3 (according to the reactions in Eqs. (1)–(4)), and eventually, they were grafted onto the CS shells.

$$Fe_3O_4 \rightarrow Fe_2O_3 + FeO \quad (1)$$

$$2CuSO_4 \rightarrow 2CuO + SO_2 + O_2 \quad (2)$$

$$2Zn(NO_2)_3 \rightarrow 2ZnO + 4NO_2 + O_2 \quad (3)$$

$$2FeSO_4 \rightarrow Fe_2O_3 + SO_3 + SO_2 \quad (4)$$

The treatment of biomass with metal oxides considerably improves pyrolytic processes. The CS-metal oxides have a significant synergistic influence on pyrolysis reactions. The resultant metal oxides promoted secondary reactions on the organic volatiles produced by the pyrolysis degradation of the CS-shells' lignin and cellulose macrostructures. The metal oxide-treated CS shells were labeled as follows: CS-ZnO, CS-Fe_2O_3, CS-CuO, and CS-Fe_2O_3/FeO.

2.2.2. Decomposition kinetic models of biomass

The FWO correlation equation (Eq. 5) was used to determine the kinetic parameters. The stoichiometry and kinetics model for isothermal devolatilization of biomass presented as Eqs. (6) and (3) respectively, was previously reported by Wang et al. [22].

$$g(\alpha) = \frac{A}{\beta} 0.00484 \exp\left(-1.052 \frac{E_\alpha}{RT}\right) \quad (5)$$

Subsequently, taking the natural log of both sides resulted in Eq. (5).

$$\ln(\beta) = \ln \frac{AE_\alpha}{Rg(a)} - 5.331 - 1.052 \frac{E_\alpha}{RT} \quad (6)$$

Where α is the extent of conversion, E_α is the activation energy and A is the pre-exponential factor. The plots of $\ln(\beta)$ against $\frac{1}{T}$ gives straight line from which activation energy, E_α is obtained and pre-exponential evaluated using solid-state reaction models. The solid-state reaction models are presented in Table 2. The best-fit model was identified using Bayesian Information Criteria (BIC). The Bayesian information criterion (BIC) (also known as the Schwarz criterion) is another statistical measure for comparative evaluation among models [23].

The BIC is determined using Eq. (7).

Table 2
Solid state reaction models from the Coat-Redfern method [3].

Mechanisms	Models g(α)
Reaction	
(R_1) First Order	-ln(1-α)
(R_2) Second Order	$(1-\alpha)^{-1}$ -1
(R_3) Third Order	[(1-α)-2 -1]/2
Diffusion	
(D_1) One-way Transport	α^2
(D_2) Two-way Transport	α+(1-α)ln(1-α)
(D_3) Three-way Transport	$1-((1-\alpha)1/3)^2$
(D_4) Ginstling-Brounshtein Eq	$1-2\alpha/3-(1-\alpha)^{2/3}$
Nucleation	
(A_4) Avarami-Erofe'ev 4	$[-\ln(1-\alpha)]^{1/4}$
Contracting	
(C_1) Area contracting	$1-(1-\alpha)^{1/2}$
(C_2) Volume contracting.	$1-(1-\alpha)^{1/3}$

$$BIC = \frac{kLn(n)}{n} - \frac{2l}{n} \tag{7}$$

The relative likelihood of the tested models was computed using Eq. (8).

$$Relative\ Likelihood = \exp(BIC_{min} - BIC_i) \tag{8}$$

where.BIC_{min} is the BIC of a model with minimum value?

BIC_i BIC of model i.

The thermodynamic parameters such as changes in enthalpy, Gibb's free energy, and entropy of the devolatilization reaction of HTS were evaluated using relationships from Eqs. (9)–(8) [2].

$$A = \frac{[\beta E exp(E_\alpha / RT_m)]}{RT_m^2} \tag{9}$$

$$\nabla H = E_\alpha - RT_m \tag{10}$$

where ∇H is change in enthalpy, E_α, activation energy, R, gas constant, and T_m is peak temperature of the DTG curve for the decomposition of HTS by pyrolysis.

$$\nabla G = E_\alpha + RT_m \ln\left(\frac{K_B T_m}{hA}\right) \tag{11}$$

$$\nabla S = \frac{\nabla H - \nabla G}{T_m} \tag{12}$$

Where ∇G is the change in Gibb's free energy for thermal decomposition of HTS, $K_B, Boltzman\ constant = 1.381 \times 10^{-23} J/K$, h, $Planck's constant = 6.626 \times 10^{-34} Js$.

3. Results and discussion

3.1. Thermogravimetric analysis of CS-shell and metal oxide-treated CS-shell

The proximal and ultimate compositions of the CS shell, including its heating value, and its pioneer devolatilization pattern have already been documented are presented in the previous study [8]. Table 3 presents the CS-shell characterization data.

The CS-shell and metal oxides-treated CS shell decompositions were then studied using thermogravimetric pyrolysis at heating rates of 10, 15, and 20C/min to assess the effect of the metal oxides on the thermo-kinetic parameters. Fig. 1(a) and (b) show the weight loss and devolatilization rate characteristics of the CS-shell and metal oxide-treated CS shells, which describe the decomposition profiles of the samples.

The TG profiles of raw CS-shell and metal oxide-treated CS shells reveal the same pattern and discrete stages of degradation. Between 30 and 220 °C, the release of around 9 wt% lighter volatiles, such as water and extractives trapped in the structure of the biomass, occurred, corresponding to volatile extractives, and water [24]. The effect of the metal oxides as catalysts is less prominent in the drying zone, yet CS-CuO exhibits peculiar behavior. The weight loss is around 8 wt% when compared to other metal oxide-treated CS shells where the CuO decreased during the drying process.

Because of the degradation of the shell macrostructure, the second stage of decomposition was rapid, resulting in a weight loss of 42.67 wt%. The Fe_2O_3/FeO-treated shell requires higher temperatures of 10 °C than the Fe_2O_3-treated shell, while the remaining ZnO and CuO-treated shells fall in the middle. The weight loss at the third stage accounts for about 8 wt% of the total weight loss, with CS-Fe_2O_3/FeO having the highest residual biochar of 38 wt% and raw CS-shell having the lowest of 25 wt%. Because of the presence of metal oxides which served as catalysts, the biochar may have a higher ash content.

Fig. 1b presents the DTG curves of the CS-shell and metal oxide-treated CS shells, which indicate the amount of vapor released per minute. The peaks between 40 and 220 °C represent dehydration. The CS-hell decomposition resulted in a maximum dehydration of 1.668 % wt./min, while that of the CS-ZnO is the least at 0.8131 % wt./min. The metal oxides suppressed the dehydration reaction, with ZnO being the most active. The peaks observed between 220 and 400 °C belong to the degradation of hemicelluloses, extractives,

Table 3
Physicochemical characteristics of CS shell.

Proximate analysis (dry basis)			Ultimate analysis (dry basis)		
Parameter (wt.%)	**Value**	*Hyphaene thebaica* shell [3],	**Parameter (wt.%)**	**Value**	*Hyphaene thebaica* shell [3],
Moisture	3.70	4.97	Carbon	51.99	42.50
Volatile matter (VM)	70.97	73.31	Hydrogen	6.00	5.50
Fixed carbon (FC)	22.37	11.96	Nitrogen	0.06	0.55
Ash content	2.96	8.75	Sulfur	0.27	1.17
HHV (MJ/kg)	18.18	21.07	Oxygen	41.68	50.30

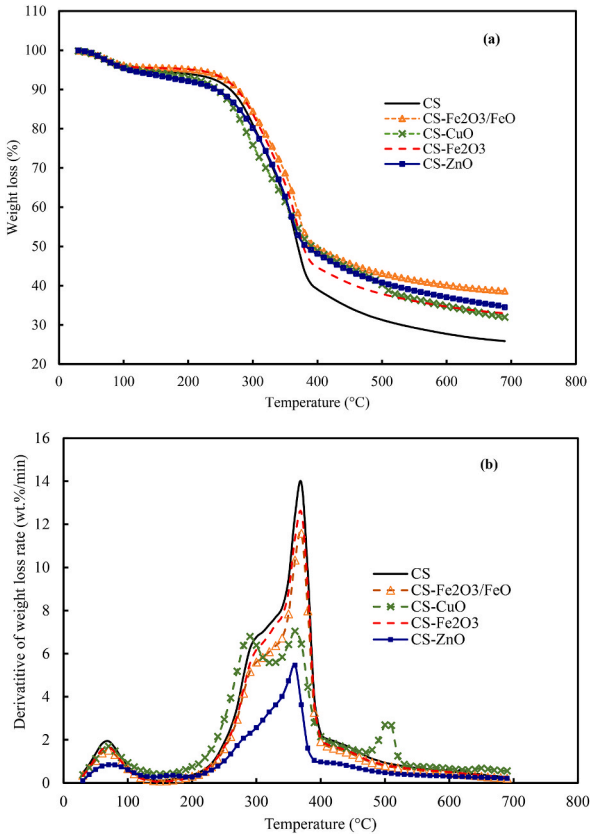

Fig. 1. Thermogravimetric curves (b) Differential thermogravimetric curves for pyrolysis of CS-Shell and metal oxide-treated CS shells.

and celluloses. ZnO suppressed devolatilization at all temperatures, with a maximum devolatilization rate of 5.461 wt%/min at 360 °C. The ZnO favors higher biochar yield suggesting an increase in aromatization of CS instead of cracking reactions [25], which involves the dehydration of methoxy and acetyl bond breakage of hemicellulose and cellulose [22] and subsequent polymerization to form a more rigid solid phase, called biochar. The ZnO-treated shell has a maximum devolatilization rate of 13.92 wt%/min at 370 °C.

Two distinctive peaks are observed in the DTG curve of the CS-Fe_2O_3 sample in the active pyrolysis zone. These differences indicate the catalytic effects of the metal oxides on the pyrolysis of CS-shell. At the final stage of the pyrolysis, the catalytic activities of Fe_2O_3 are more pronounced as more degradation of the residue occurs to liberate more vapor (2.67 % wt.%/min), which might contribute to the yield of vapor phase products. The Fe_2O_3 particle has a catalytic effect on the degradation of the char because of the breakdown of the residual molecular structure of the biochar. This shows that the Fe_2O_3 has better interaction with biomass, which enhances the catalytic degradation of the biomass compared to the Fe_2O_3/FeO. However, the increase in peak points indicates the complex, multi-step reactions of the catalytic reaction system [12].

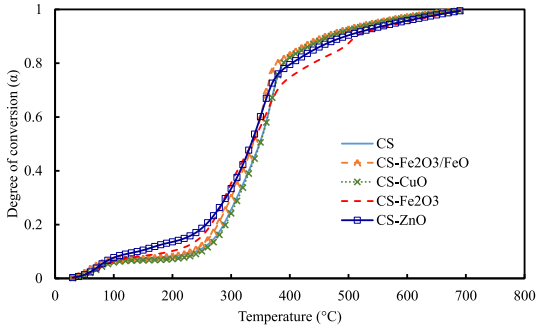

Fig. 2. Conversion, α vs temperature curve for pyrolysis of CS-Shell and metal oxide-treated CS shells.

3.2. Evaluation of the kinetics parameters of metal oxide-treated CS shells pyrolysis

The solid-state reaction mechanisms to describe pyrolysis reactions follow the criteria of the kinetics committee of the International Confederation for Thermal Analysis and Calorimetry (ICTAC), which suggested that the extent of conversion versus temperature curve be examined [26]. The curves for the CS-shell and metal oxide-treated CS shells under analysis are presented in Fig. 2. The curves resulted in a sigmoid shape, which rules out the use of power law models, which simulate accelerating and decelerating processes [25].

The kinetic characteristics of CS-shell and metal oxide-treated CS shells thermogravimetric data acquired at three different heating rates (10, 15, and 20C/min) were analyzed and predicted. The plots of the thermogravimetric decomposition of CS, CS-Fe_2O_3/FeO, CS-Fe_2O_3, CS-CuO, and CS-ZnO in the active pyrolysis zone (220–400 °C) with conversion ranging from 0.1 to 0.9 at the three heating rates are shown in Fig. 3a–e. The plots are linear with a change in slope, from which the E_α was calculated at each degree of conversion. The R-square values of the plots are presented in Table 4.

Furthermore, mechanisms of the solid-state models (Table 2) that describe the pyrolysis reactions were determined using Bayesian information criteria (BIC). The effective mechanisms that govern the CS-shell and metal oxide-treated CS shell pyrolysis reactions are established through the FWO method using the BIC approach. The BIC gives reliable results because of its minimum error in the activation energy (E_α) and pre-exponential factor. Fig. 4 shows the reaction models and the accompanying relative probability generated using BIC. The Gistling-Brounstein diffusion (D4) has the lowest BIC values and a relative likelihood of one (1), which suggests the pyrolysis reaction follows the diffusion reaction pathways. The mechanisms of the C1 and C2 contraction and the D1, D2, and D3 diffusion have a significant combined effect on controlling the pyrolysis reactions. Therefore, the diffusion and contraction model mechanisms control the pyrolysis decomposition reaction for the CS-shell and metal oxide-treated CS-shell. Similarly, the pyrolysis decomposition of *Typha latifolia* obeys the mechanisms of contraction and diffusion [6].

Fig. 5 and Table 5 present the variation of E_α for pyrolysis of CS-shell and metal oxide-treated CS-shell obtained from the FWO

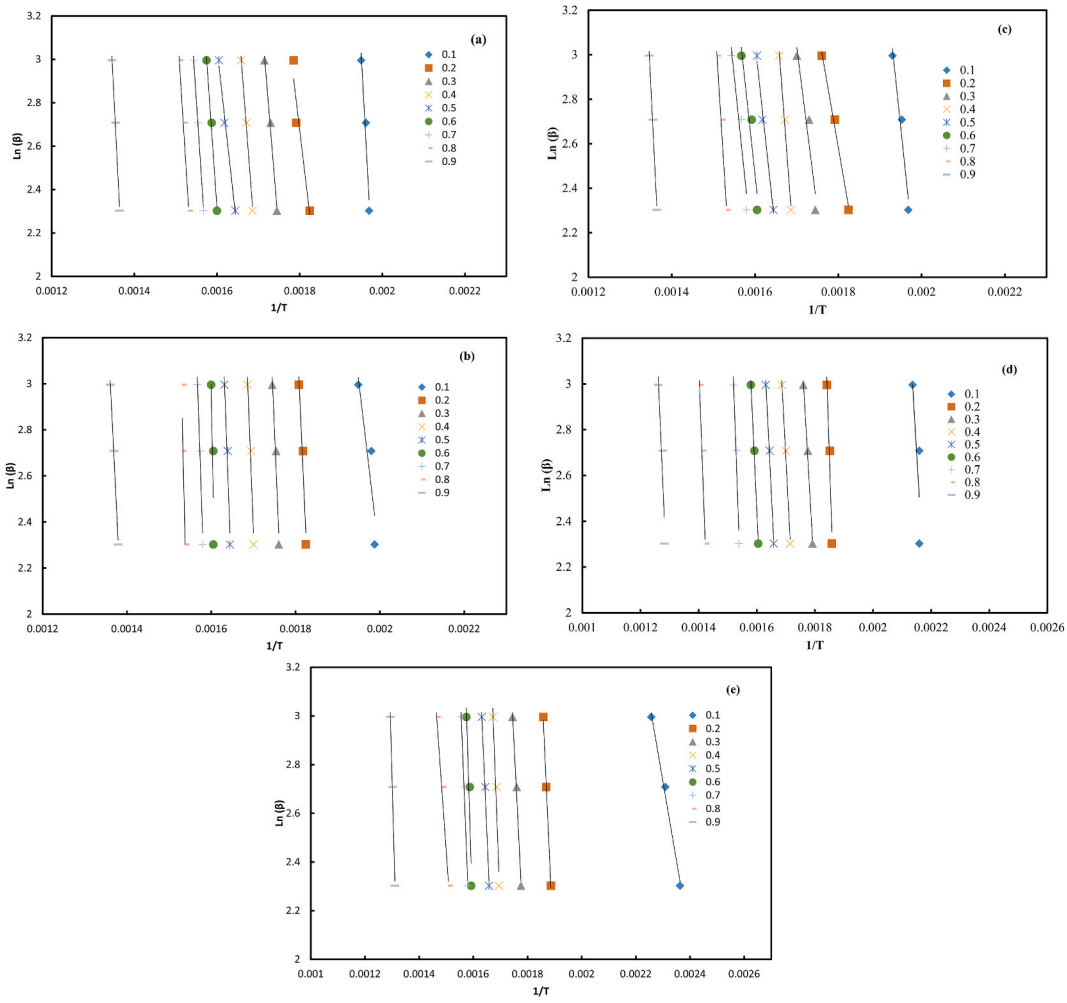

Fig. 3. Linear plots of FWO for (a) CS-Shell, (b) CS- Fe_2O_3/FeO, (c) CS-CuO, (d) CS- Fe_2O_3, (e), CS-ZnO pyrolysis at 10, 15 and 20 °C/min heating rates.

Table 4
The R-squared values of FWO plots.

R2					
α	**CS**	**CS-Fe2O3/FeO**	**CS-CuO**	**CS-Fe_2O_3**	**CS-ZnO**
0.1	0.988	0.828	0.988	0.923	0.993
0.2	0.983	0.956	0.992	0.965	0.998
0.3	0.991	0.978	0.996	0.996	0.991
0.4	0.941	0.966	0.991	0.992	0.986
0.5	0.990	0.956	0.990	0.995	0.994
0.6	0.991	0.967	0.986	0.991	0.981
0.7	0.991	0.956	0.993	0.985	0.993
0.8	0.993	0.978	0.991	0.991	0.994
0.9	0.992	0.992	0.994	0.985	0.993

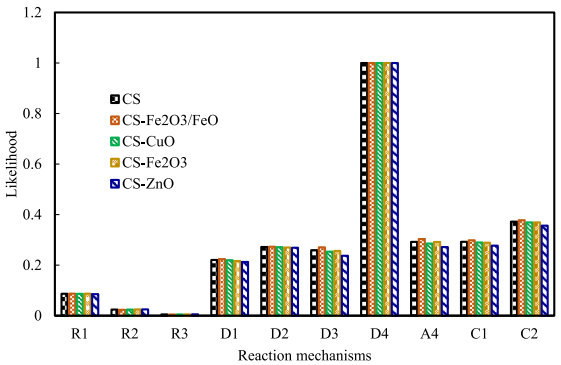

Fig. 4. Relative likelihood of models that govern the thermogravimetric pyrolysis of CS-shell and metal oxide-treated CS shells.

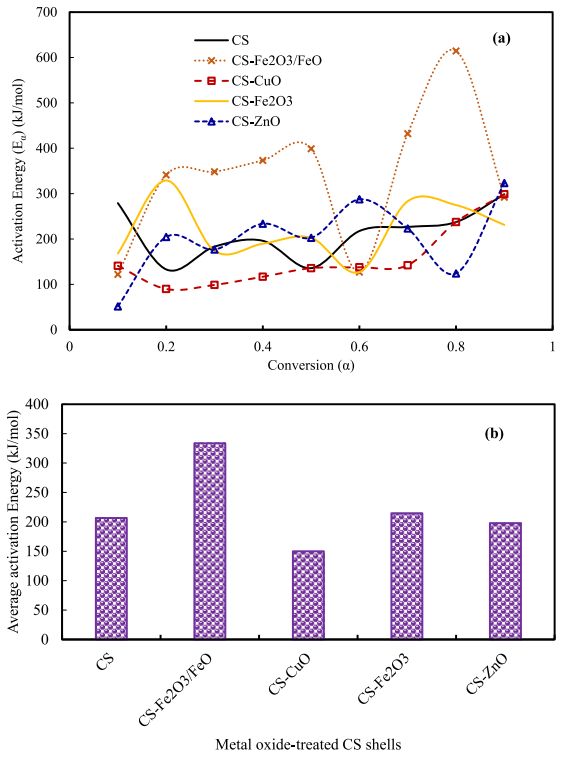

Fig. 5. Variation of (a) E_α with the degree of conversion (α) and (b) E_α for pyrolysis of CS-shell and metal-oxide treated CS Shells.

Table 5
Activation energy and frequency factors for CS-shell and metal oxide treated CS shells thermogravimetric pyrolysis from FWO method.

α	CS		CS-Fe2O3/FeO		CS-CuO	CS-Fe_2O_3		CS-ZnO			
	Eα (kJ/mol)	A (s-1)	Eα (kJ/mol)	A (s-1)	Eα (kJ/mol)	A (s-1)		Eα (kJ/mol)	A (s-1)	Eα (kJ/mol)	A (s-1)
0.1	278.98	2.71E+17	122.07	48920.54	140.96	1673374.00		168.07	266228155.60	51.42	2.79E+17
0.2	133.02	378289.98	341.24	3.09E+22	89.81	117.26		328.96	3.11E+21	204.47	378289.98
0.3	183.18	44863546	348.36	1.17E+23	98.91	642.88		173.79	776207311	176.89	4486354562
0.4	196.07	49981097469.00	373.19	1.22E+25	116.83	18334.98		189.57	14831239467	233.75	49981097469
0.5	135.74	629022.5060.00	398.88	1.48E+27	135.73	629022.50		202.67	1.71E+11	202.67	629022.51
0.6	217.60	2.81E+12	127.06	124130.35	137.78	923753.10		127.05	124130.34	287.49	2.81E+12
0.7	226.68	1.53E+13	432.21	7.54E+29	142.18	2101083.00		283.31	6.09E+17	223.17	1.53E+13
0.8	237.37	1.13E+14	614.49	4.82E+44	237.36	1.13E+14		274.79	1.24E+17	124.18	1.13E+14
0.9	298.56	1.05E+19	292.13	3.17E+18	298.56	1.06E+19		231.02	3.45E+13	323.33	1.06E+19
Average	211.91	1.20E+18	338.85	5.35E+43	155.35	1.17E+18		219.92	3.46E+20	203.04	1.20E+18

method. The E_α for the CS-shell and metal oxides-treated CS shells vary with α (from 0.1 to 0.9) due to the complex and multi-step nature of the pyrolysis reactions [12,25]. In particular, the activation energies of CS-shell range between 133 and 298 kJ/mol. The large difference in the E_α values occurred from the complexity and multi-step reactions of pyrolysis degradation of the intertwined lignin, cellulose, and hemicellulose structure of the biomass [24,27]. On treating CS shells with the ZnO, CuO, Fe_2O_3/FeO, and Fe_2O_3, the E_α varies in contrast to that of the Cs-shell pyrolysis decomposition as shown in Table 5. This reveals that the metal oxides during the pyrolysis increase the complexity of the pyrolysis reactions through secondary reactions on the vapor. The variations in the ranges of E_α indicate that the metal oxides serving as catalysts altered the reaction pathways in different mechanisms, as revealed by the DTG curves, where peaks of vapor evolution vary.

Because of the degradation of lignin into biochar, the E_α are high when α is between 0.7 and 0.9 [3] due to the high thermal stability of lignin [28], irrespective of whether CS-shell is treated with metal oxide or not. The ZnO-treated CS-shell with exhibited a distinct pattern, as there is a decrease in E_α for conversion ranging between 0.6 and 0.8.

Fig. 5b presents the average E_α of the thermogravimetric pyrolysis of CS-shell and metal oxide-treated CS shells. The E_α for CS, CS-Fe_2O_3/FeO, CS-CuO, CS-Fe_2O_3, and CS-ZnO are 211.91, 338.85, 155.35, 219.92, and 203.04 kJ/mol, respectively. The CuO and ZnO reduce the E_α from 211 kJ/mol of the Cs-shell to 155 kJ/mol and 203 kJ/mol, respectively. The metal oxides as catalysts interact with volatiles after bond breakage of the CS-shell macrostructure and promote secondary reactions on the high molecular weight compounds. This finding conforms to the one reported in the literature [10,29]. However, the E_α for the shells treated with $FeSO_4$ and Fe_3O_4 first decomposed into Fe_2O_3 and Fe_2O_3/FeO, increasing the E_α from 211 to 338 kJ/mol and 219 kJ/mol, respectively, higher than that of the CS, CuO, and ZnO-treated CS-shell pyrolysis [30].

3.3. Thermodynamics parameters for CS-shell and metal oxide-treated CS-shell under thermogravimetric pyrolysis

The profiles of variations in change in enthalpy, ΔH, with the degree of conversion of the CS-shell, CS-Fe_2O_3/FeO, CS-Fe_2O_3, CS-CuO, and CS-ZnO and their corresponding average values are presented in Fig. 6a and b, respectively.

The heat energy absorbed (Enthalpy, H) devolatilized the CS shell through structural bond breakage and caused weight loss from the release of vapor, which condenses to pyrolytic bio-oil. The change in Enthalpy (ΔH) varies with α (0.1–0.9) as depicted in Fig. 6a is positive for all the decomposition of CS-shell and metal oxide-treated CS shells. The average ΔH shown in Fig. 6b at 206.56, 333.58, 150, 214.65, and 197.78 kJ/mol are for the CS, CS-Fe_2O_3/FeO, CS-CuO, CS-Fe_2O_3, and CS-ZnO degradations, respectively. These results established endothermic reactions prevailed in the entire degradation reactions in the active pyrolysis zone, this conforms to the findings reported in the literature [15]. The CS-Fe_2O_3/FeO and CS-Fe_2O_3 decomposed with the highest average ΔH, which indicates that more energy is absorbed to propagate the pyrolysis degradation reactions. This is due to the energy absorbed to decompose the $FeSO_4$ to Fe_2O_3 and the IOD into the mixed iron oxides (Fe_2O_3/FeO), which are required to catalyze the pyrolysis secondary degradation reactions [18]. However, the average ΔH of the CS-CuO is 150 kJ/mol, which is less than the 206 kJ/mol required for the CS-shell. A similar finding was reported by Ling et al. [15] for the pyrolysis of palm kernel shells and plastic wastes. In addition, there was a slight decrease in the ΔH of CS-ZnO to 197 kJ/mol compared to 206 kJ/mol required for the CS shell. The reduction in the ΔH is due to the ease of decomposing $Zn(NO_3)_2$ to ZnO during the pyrolysis thermal decomposition [31].

The pattern of change in Gibb's free energy (ΔG) with the α of CS-shell, CS- Fe_2O_3/FeO, CS-Fe_2O_3, CS-CuO, and CS-ZnO and the corresponding average ΔG are presented in Fig. 7a and b. Gibb's free energy decreases with the degree of conversion towards biochar formation for the CS-shell and metal oxide-treated CS-shell. This trend was reported in a study [32,33]. The ΔG has positive values for α (0.1–0.8) for CS-ZnO, 0.2 to 0.6 for CS-shell and CS-CuO, 0.3 to 0.7 for CS- Fe_2O_3, and 0.1 to 0.2 and 0.6 to 0.7 for CS-Fe_2O_3/FeO. The values of the ΔG established that the reaction is non-spontaneous, which indicates that external thermal energy is needed for the pyrolysis reaction to occurs. Outside these ranges, the ΔG is negative, which establishes that the decomposition is spontaneous at those temperatures associated with the thermal inertia of the catalysts, which influences the pyrolysis reactions. The CS-shell treated with Fe species such as CS-Fe_2O_3 and CS-Fe_2O_3/FeO has more reversibility and equilibrium tendency than CuO and ZnO-treated CS shells. The average ΔG of pyrolysis for CS-Fe_2O_3 and CS-Fe_2O_3/FeO are 2 and 116 kJ, respectively.

Furthermore, the change in entropy (ΔS) varies with α and type of metal oxide used in the treatment of the CS Shells, as presented in Fig. 8. The ΔS is positive throughout the decomposition process, from 0.1 to 0.9, except for CS-CuO, which has a negative ΔS between 0.2 and 0.4. The variations of ΔS with α establish the complex nature of the thermogravimetric pyrolysis of the CS-shell and metal oxide-treated CS shells. The ΔS of CS and CS-ZnO follow a similar trend, which decreases as the α increases from 0.1 to 0.2. The decrease in ΔS might be due to the evolution of volatiles, mostly water vapor, which reduces the degree of disorderliness. However, the ΔS of those CS shells treated with IOD and $FeSO_4$ salts, CS-Fe_2O_3/FeO and Fe_2O_3 respectively, increases from 0.1 to 0.5 due to thermal inertia, which releases more heat to the vapor, thus with the high degree of disorderliness. At 0.6 degrees of conversion, the release of volatiles increased eventually lower the degree of disorder [12]. The value of ΔS is positive at the 0.6 conversion degree, but the ΔS has decreased drastically. This is because of the increased rate of decomposition of the CS-shell macrostructure, which releases more volatiles and decreases the degree of disorderliness of the vapor molecules.

4. Conclusion

1. The degradation behavior of CS-shell and metal oxide-treated CS-shell samples was examined using TGA up to 800 °C under 10, 15, and 20 °C/min heating rates. Peak maximum temperatures shifted by about 5 °C as heating rates increased. The DTG curve analysis revealed unique decomposition patterns having characteristic peaks. The peaks were observed between 350 and 380 °C, with significant degradation taking place between 200 and 600 °C.

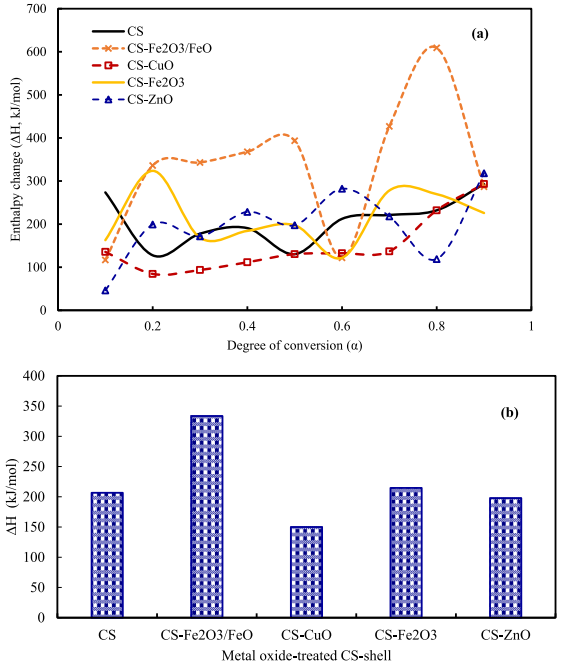

Fig. 6. Variation of (a) ΔH with the degree of conversion (α) and (b) ΔH for pyrolysis of CS-shell and metal-oxide treated CS Shells.

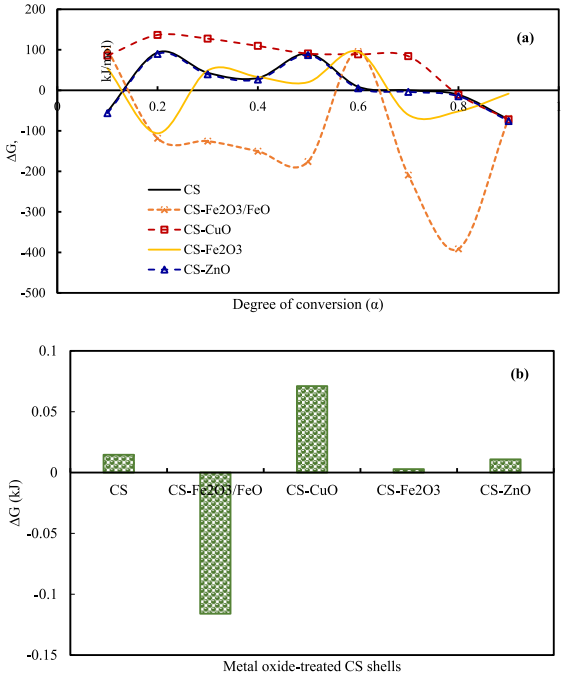

Fig. 7. Variation of (a) ΔG with the degree of conversion (α) and (b) Average ΔG for pyrolysis of CS-shell and metal-oxide treated CS Shells.

2. The activation energies for pyrolysis of CS shells treated with ZnO, CuO, Fe_2O_3, and Fe_2O_3/FeO are 118.15, 142.81, and 139.56 kJ/mol, respectively differ from CS shell pyrolysis. As a result, the metal oxide altered various pyrolysis reactions propagated by the Gistling-Brounshtein model's diffusion-controlled mechanism, as determined by Bayesian information criteria.
3. The study provides kinetics and thermodynamics parameters for pyrolysis of CS shells treated with ZnO, CuO, Fe_2O_3, and Fe_2O_3/FeO that are not well documented in the literature.

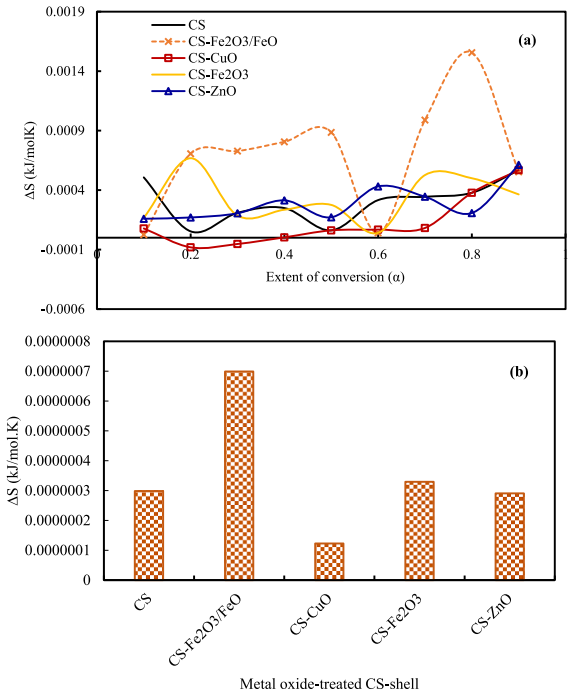

Fig. 8. Variation of (a) ΔS with a degree of conversion (α) and (b) ΔS for pyrolysis of CS-shell and metal-oxide treated CS-Shell.

4. The kinetic models for the metal oxide-treated CS shell demonstrated excellent fitting performance, with R^2 values ranging up to 0.99. This suggested that kinetic modeling has the potential to be an effective tool for evaluating complex degradation processes, thus paving the way for new avenues of research into biomass utilization.
5. The kinetic modeling results based on the TGA/DTG analyses revealed the understanding of metal oxide-treated CS-shell decomposition, which can inform the development of efficient thermochemical conversion systems.
6. The study advocates for the extensive use of different metal oxides, especially those obtained from readily available iron ore dust, in the catalytic pyrolysis of CS shells for bioenergy and chemical recovery.

Data availability

Data will be made available on request.

CRediT authorship contribution statement

Kabir Garba: Writing – review & editing, Writing – original draft, Supervision, Methodology, Investigation, Formal analysis, Data curation, Conceptualization. **Habu Iyodo Mohammed:** Writing – review & editing, Writing – original draft, Methodology, Investigation, Formal analysis, Conceptualization. **Yusuf Makarfi Isa:** Writing – review & editing, Methodology, Investigation, Formal analysis, Conceptualization.

Declaration of competing interest

There are no competing financial or personal interests that could have appeared to affect the study reported in the research paper.

Acknowledgments

The authors acknowledge the research grants provided by the Tertiary Education Trust (TETFund) of Nigeria, under the Institutional Based Research grant (IBR) (Project No: TETFund/DR&D/CE/IBR/2023) that resulted in this article.

References

[1] M. Jia, B. Fong, A. Chun, M. Loy, B. Lai, F. Chin, M.K. Lam, S. Yusup, Z. Abbas, Catalytic pyrolysis of Chlorella vulgaris : kinetic and thermodynamic analysis, Bioresour. Technol. 289 (2019) 121689, https://doi.org/10.1016/j.biortech.2019.121689.

[2] C. Zhang, C. Wang, R. Tao, J. Ye, Thermal stability and thermal decomposition kinetics of Ginkgo biloba leaves waste residue, Therm. Sci. 22 (2018) 1059–1069, https://doi.org/10.2298/TSCI170117154Z.

[3] H.I. Mohammed, K. Garba, S.I. Ahmed, L.G. Abubakar, Thermodynamics and kinetics of Doum (Hyphaene thebaica) shell using thermogravimetric analysis : a study on pyrolysis pathway to produce bioenergy, Renew. Energy 200 (2022) 1275–1285, https://doi.org/10.1016/j.renene.2022.10.042.

[4] M.A. Islam, M. Auta, G. Kabir, B.H. Hameed, A thermogravimetric analysis of the combustion kinetics of karanja (Pongamia pinnata) fruit hulls char, Bioresour. Technol. 200 (2016) 335–341, https://doi.org/10.1016/j.biortech.2015.09.057.

[5] Z. Ma, D. Chen, J. Gu, B. Bao, Q. Zhang, Determination of pyrolysis characteristics and kinetics of palm kernel shell using TGA – FTIR and model-free integral methods, Energy Convers. Manag. 89 (2015) 251–259, https://doi.org/10.1016/j.enconman.2014.09.074.

[6] M.S. Ahmad, M.A. Mehmood, S.T.H. Taqvi, A. Elkamel, C.G. Liu, J. Xu, S.A. Rahimuddin, M. Gull, Pyrolysis, kinetics analysis, thermodynamics parameters and reaction mechanism of Typha latifolia to evaluate its bioenergy potential, Bioresour. Technol. 245 (2017) 491–501, https://doi.org/10.1016/j.biortech.2017.08.162.

[7] I. Jia, Y. Tan, A. Chun, M. Loy, B. Lai, F. Chin, K. Wai, Green Technologies and Sustainability Co-pyrolysis of Chlorella vulgaris with plastic wastes : thermal degradation , kinetics and Progressive Depth Swarm-Evolution (PDSE) neural network-based optimization, Green Technol. Sustain 2 (2024) 100077, https://doi.org/10.1016/j.grets.2024.100077.

[8] K. Garba, I. Yakub, Y. Makarfi, L. Garba, Y. Abdalla, B.H. Hameed, Heliyon Pyrolysis of Canarium schweinfurthii hard-shell : thermochemical characterisation and pyrolytic kinetics studies, Heliyon 9 (2023) e13234, https://doi.org/10.1016/j.heliyon.2023.e13234.

[9] W.A. Wibowo, R.B. Cahyono, R. Rochmadi, A. Budiman, Kinetics of in-situ catalytic pyrolysis of rice husk Pellets using a multi-Component kinetics, Model 18 (2023) 85–102, https://doi.org/10.9767/bcrec.17226.

[10] W. Agung, R. Bakti, A. Budiman, Thermogravimetric analysis and kinetic study on catalytic pyrolysis of rice husk pellet using its ash as a low-cost in-situ, Catalyst 11 (2022) 207–219, https://doi.org/10.14710/ijred.2022.41887.

[11] Y. Yee, C. Hoon, K. Ng, L. Yee, L. Suyin, G. Suchithra, T. Gopakumar, Kinetics and mechanisms for catalytic pyrolysis of empty fruit bunch fibre and cellulose with oxides, SN Appl. Sci. 2 (2020) 1–14, https://doi.org/10.1007/s42452-020-03249-1.

[12] D. Kin, W. Gan, A. Chun, M. Loy, B. Lai, F. Chin, S. Yusup, P. Unrean, E. Rianawati, M.N. Acda, Bioresource Technology Kinetics and thermodynamic analysis in one-pot pyrolysis of rice hull using renewable calcium oxide based catalysts, Bioresour. Technol. 265 (2018) 180–190, https://doi.org/10.1016/j.biortech.2018.06.003.

[13] H. Yang, G. Ji, P.T. Clough, X. Xu, M. Zhao, Kinetics of catalytic biomass pyrolysis using Ni-based functional materials, 195, https://doi.org/10.1016/j.fuproc.2019.106145, 2019.

[14] M. Guida, H. Bouaik, E.M. L, A. Moubarik, A. Aboulkas, K. El harfi, A. Hannioui, Utilization of Starink approach and avrami theory to evaluate the kinetic parameters of the pyrolysis of olive mill solid waste and olive mill wastewater, J. Adv. Chem. Eng. 7 (2017) 1–8, https://doi.org/10.4172/2090-4568.1000155.

[15] A. Ling, K. Chee, B. Lai, F. Chin, S. Meng, X. Goh, Y. Ho, A. Chun, M. Loy, K. Wai, C. Loong, S. Sow, M. Lock, Thermo-catalytic co-pyrolysis of palm kernel shell and plastic waste mixtures using bifunctional HZSM-5/limestone catalyst : kinetic and thermodynamic insights, J. Energy Inst. 107 (2023) 101194, https://doi.org/10.1016/j.joei.2023.101194.

[16] H. Persson, I. Duman, S. Wang, L.J. Pettersson, W. Yang, Catalytic pyrolysis over transition metal-modified zeolites: a comparative study between catalyst activity and deactivation, J. Anal. Appl. Pyrolysis (2018), https://doi.org/10.1016/j.jaap.2018.12.005.

[17] P. He, W. Shan, Y. Xiao, H. Song, Performance of Zn/ZSM-5 for in situ catalytic upgrading of pyrolysis bio-oil by methane, Top. Catal. (2015), https://doi.org/10.1007/s11244-015-0508-4.

[18] Y. V Lugovoy, K. V Chalov, Y.Y. Kositsov, E.M. Sulman, G. Mikhail, Pyrolysis of Agricultural Waste in the Presence of Fe-Subgroup Metal-Containing Catalysts, vol. 76, 2019, pp. 1453–1458, https://doi.org/10.3303/CET1976243.

[19] H. Xia, X. Yan, S. Xu, L. Yang, Y. Ge, J. Wang, S. Zuo, Effect of Zn/ZSM-5 and FePO 4 Catalysts on Cellulose Pyrolysis, 2015, p. 2015.

[20] V. Savou, S. Kumagai, Y. Saito, T. Kameda, T. Yoshioka, Effects of acetic acid pretreatment and pyrolysis temperatures on product recovery from Fijian sugarcane bagasse, Waste and Biomass Valorization (2019), https://doi.org/10.1007/s12649-019-00866-9.

[21] M. Jabłońska, M. Rachwał, M. Wa, M.K. Gaweł, E. Teper, Mineralogical and Chemical Specificity of Dusts Originating from Iron and Non-ferrous Metallurgy in the Light of Their Magnetic Susceptibility, 2021, pp. 1–20.

[22] P. Wang, B.H. Howard, Impact of thermal pretreatment temperatures on woody biomass chemical composition, physical properties and microstructure, Energies 11 (2018) 1–20, https://doi.org/10.3390/en11010025.

[23] J. Chen, X. Fan, B. Jiang, L. Mu, P. Yao, H. Yin, X. Song, Pyrolysis of oil-plant wastes in a TGA and a fixed-bed reactor : thermochemical behaviors , kinetics , and products characterization, Bioresour. Technol. 192 (2015) 592–602, https://doi.org/10.1016/j.biortech.2015.05.108.

[24] C.L. Waters, R.R. Janupala, R.G. Mallinson, L.L. Lobban, Staged thermal fractionation for segregation of lignin and cellulose pyrolysis products: an experimental study of residence time and temperature effects, J. Anal. Appl. Pyrolysis 126 (2017) 380–389, https://doi.org/10.1016/j.jaap.2017.05.008.

[25] S. Vyazovkin, A.K. Burnham, L. Favergeon, N. Koga, E. Moukhina, L.A. Pérez-maqueda, N. Sbirrazzuoli, Thermochimica Acta ICTAC Kinetics Committee recommendations for analysis of multi-step kinetics, Thermochim. Acta 689 (2020) 178597, https://doi.org/10.1016/j.tca.2020.178597.

[26] S. Vyazovkin, A.K. Burnham, J.M. Criado, L.A. Pérez-maqueda, C. Popescu, N. Sbirrazzuoli, Thermochimica Acta ICTAC Kinetics Committee recommendations for performing kinetic computations on thermal analysis data, Thermochim. Acta 520 (2011) 1–19, https://doi.org/10.1016/j.tca.2011.03.034.

[27] G. Kabir, B.H. Hameed, Recent progress on catalytic pyrolysis of lignocellulosic biomass to high- grade bio-oil and bio-chemicals, Renew. Sustain. Energy Rev. 70 (2016) 945–967, https://doi.org/10.1016/j.rser.2016.12.001.

[28] F. Surahmanto, H. Saptoadi, H. Sulistyo, T.A. Rohmat, Effect of heating rate on the slow pyrolysis behaviour and its kinetic parameters of oil-palm shell, Int. J. Renew. Energy Res. 7 (2017) 1138–1144.

[29] Y. Zheng, J. Wang, C. Liu, Y. Lu, X. Lin, W. Li, Z. Zheng, Catalytic copyrolysis of metal impregnated biomass and plastic with Ni-based HZSM-5 catalyst : synergistic effects , kinetics and product distribution, Int. J. Energy Res. 44 (2020) 5917–5935, https://doi.org/10.1002/er.5370.

[30] N. Kanari, N.E. Menad, E. Ostrosi, S. Shallari, F. Diot, E. Allain, J. Yvon, Thermal behavior of hydrated iron sulfate in various atmospheres, Metals 8 (2018) 1–9, https://doi.org/10.3390/met8121084.

[31] Q. Lu, Z.F. Zhang, C.Q. Dong, X.F. Zhu, Catalytic upgrading of biomass fast pyrolysis vapors with nano metal oxides: an analytical Py-GC/MS study, Energies 3 (2010) 1805–1820, https://doi.org/10.3390/en3111805.

[32] T. Li, A. Chun, M. Loy, B. Lai, F. Chin, J. Yau, H. Alhamzi, Y. Ho, C. Loong, K. Wai, M. Xin, J. Wee, M. Kee, Z. Abbas, S. Yusup, S. Sow, M. Lock, Synergistic effects of catalytic co-pyrolysis Chlorella vulgaris and polyethylene mixtures using artificial neuron network : thermodynamic and empirical kinetic analyses, J. Environ. Chem. Eng. 10 (2022) 107391, https://doi.org/10.1016/j.jece.2022.107391.

[33] Q. Wang, H. Song, S. Pan, N. Dong, X. Wang, S. Sun, Initial pyrolysis mechanism and product formation of cellulose : an Experimental and Density functional theory (DFT) study, Sci. Rep. (2020) 1–18, https://doi.org/10.1038/s41598-020-60095-2.